Research Paper
International Journal of Aerospace System Engineering
Vol.4, No.1, pp.13-21 (2017)

ISSN 2383-4986
EISSN 2508-7169
https://doi.org/10.20910/IJASE.2017.4.1.13

Performance Analysis Model for Flap Actuation System using MATLAB/Simulink

Hyunjun Cho[1,†], Choonshik Joo[1], Kilyeong Kim[1], Sangjoon Park[1]
[†]*Aerospace R&D center, Hanwha Corporation/Machinery*
KOREA
[†]*E-mail:chohjw@hanwha.com*

Abstract

In this paper, we present some results on performance analysis for flap actuation system of aircraft. For this, by utilizing MATLAB/Simulink solution, which is widely used physical model-based design tool, we particularly construct the architecture of the analysis model consisting of the main three phases: 1)commanding and outer-controlling the flap angle through flight control computer; 2)generating hydraulic/mechanical power through control module and power drive unit; 3)transmitting torque and actuating the flap through torque tube and rotary geared actuators. For mimicking the motion of the actual flap, we apply each mechanical component, which is already being used in actual aircraft, to our performance analysis model so that it guarantees the congruency of the simulation results. That is, we reflect the actual specifications of flap hardware and software as parameters of the model. Finally, simulation results are presented to illustrate the model.

Key Words : Flap actuation system, Flight control computer, Main control valve, Torque tube, Rotary geared actuator, Linear force motor, Fail-safe, Aircraft, Feedback control, Model-based design, Functional mock-up interface, MATLAM, Simulink

1. Introduction

Flap is a secondary flight control of the aircraft, which is attached to the outside of the aircraft flaperon to change the drag and lift force acting on the wing during takeoff and landing. When landing the aircraft, lowering the flap increases the camber and Angle of Attack (AOA) of the wing, allowing a landing approach at a deeper descent angle. [1]

To operate the aircraft flap normally in the presence of disturbance during flight, it is necessary to control at the system level. So far, there have been many attempts to control flaps at the system level. [2-4] In the recent years, FBW (Fly by wire) has been used to control aircraft flap in place of existing mechanical steering. [5] When the flap angle is transmitted to flight control computer (FLCC) by the wire, it detects the error at the desired flap position and performs the flap control. In this paper, we present a flight control system embedded in actual aircraft.

Although there are many applications to control the entire flap using electricity as a power source, for practical reasons, most of the aircraft to date have used hydraulic pressure as a power source. After the control command is applied to the electric motor of the hydraulic valve, once delivered, the hydraulic valve adjusts the flow rate according to the displacement of the valve stroke. This regulated flow rate thus generates torque by rotating the hydraulic

Received: June 02, 2017 Revised: June 21, 2017
Accepted: June 21, 2017
† Corresponding Author
Tel: +82-41-538-7957, E-mail: chohjw@hanwha.com

Fig. 1 Flap Actuation System

motor. In this paper, we will deal with a general flap application that uses a linear force motor, a main control valve (MCV), and a fixed displacement hydraulic motor to control flow and generate torque.

The torque generated by the hydraulic domain is amplified through the designed gear, which considers the several system requirements for speed/torque, and the torque is transmitted to the flap tip through the torque tube. Also, at the middle of each torque tube, rotary geared actuators (RGAs) for driving the actual flap are located to support and actuate the flap.

Since the surface load of actual flap is very large, it is necessary to consider sufficient margin. At this time, the RGAs should have sufficient stiffness to prevent deformation and destruction of the flap. In this paper, we will present an initial model of a torque tube and RGA that transmit torque to the flap surface for getting the meaningful results of the whole system.

Meanwhile, if there are any problems in the parts of aircraft, it may lead to a major accident, so there must be redundancy to guarantee the normal operation of the entire system. Thus, this 'fail-safe' function is present redundantly throughout the electronic-hydraulic-mechanical domain of the flap and dual or triplex redundancy of electrical components is also applied for safety. These allow the aircraft to fly normally even if some parts fail or malfunction.

The above description is being generally applied to fighter/civilian aircraft. However, despite the fact that the design based on performance analysis (i.e., model based design or model-based engineering [6-10]) is important in the initial design, due to the confidentiality of the contents based on the specialty of military business, the contents about the performance analysis model of the actual flap drive system can't be found. Therefore, the contribution of this study is as follows. 1) A performance analysis model of actual aircraft flap system is presented; 2) Flap drive system as a whole system is presented; 3) The results of applying each component to the Simulink model by mathematical generalization are presented.

The rest of the paper is organized as follows. First, Section 2 summarizes the electro-hydraulic-mechanical domain and power flow over a typical flap drive system. Also, Section 3 shows the modeling of the closed loop flap control command of the actual flight control system, and Section 4 presents not only the hydraulic power generation but also its mathematical expressions and a simplified model about power transmission. In Section 5, the simulation results will be shown to ensure the properness of our performance analysis model. Finally, we will present a summary of the results and future work in Section 6.

2. Preliminaries

2.1. Feedback Control of the Flap System

This Section describes the overall flap actuation system, which has multiple physical domains as shown in Fig.2. The feedback loop for controlling the flap system consists of a high and low-level unit loop, which represents an outermost control loop for position control of the flap, and an inner control loop for controlling the linear displacement of the hydraulic valve spool respectively. Since the general performance analysis examines the performance of the system-level controller, the lowest-level controller for the rigidity of the hardware itself can be omitted. However, in order to analyze the microscopic performance of an aircraft, it should be considered even though it's a trivial effect. For position sensing, Rotary Variable Differential Transformer (RVDT) is use and the control of flap position is performed by the difference between the input angle delivered to the reference and the flap angle from the RVDT. Here, RVDT measurements at two different locations are transferred to the FLCC to ensure the accuracy of the sensor measurements, and the FLCC guarantees the accuracy of the flap position by continually comparing these two flap position sensor values. The one is located at a power drive unit, which is a module for producing and delivering power, and another is located at a flap tip. Considering gear installation during power transmission process, the difference between these two RVDT measurements is calibrated by FLCC.

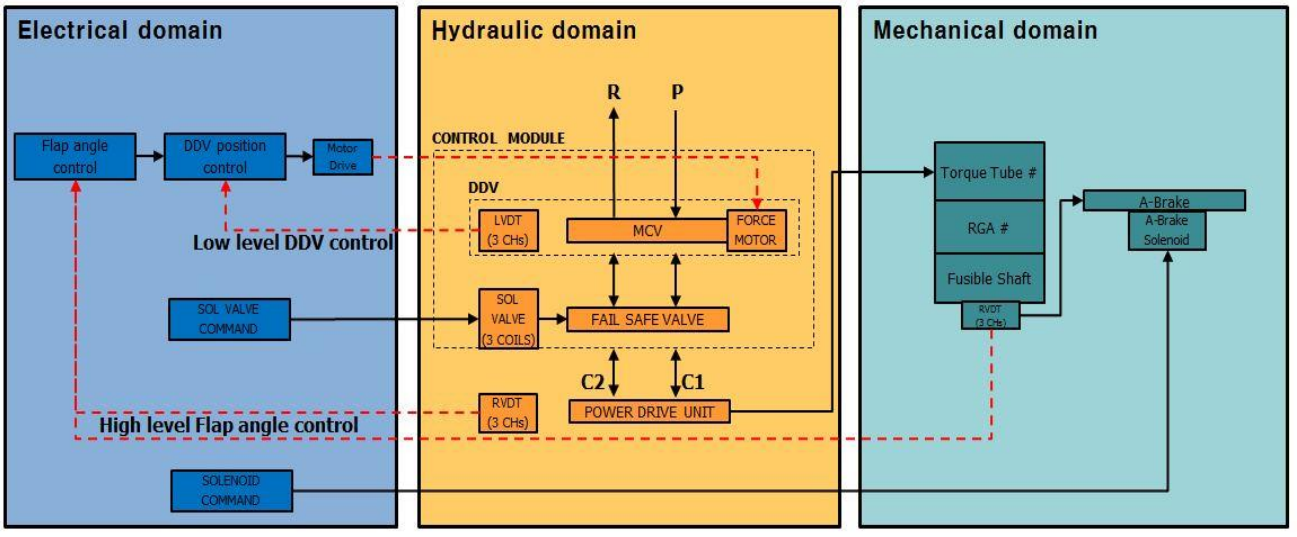

Fig. 2 Multiple Physical Domain (Flap Actuation System Schematic)

Along with the RVDT, for a low-level control, the LVDT (Linear Variable Differential Transformer) attached to the end of MCV is used to control the linear displacement of the MCV spool. Note that both control loops commonly adjust the current into the force motor. Namely, the high-level and low-level control loops consist of a simple structure in which the control layers are all located in the FLCC, although the each control layer is different.

2.2. Signal and Power Flow for Flap Control

The signal and power flows are roughly as follows. FLCC receives the analog output of RVDT and LVDT, and calculates the control amount to drive MCV, and also generates the driving current input to drive the valve. Then, direct drive valve (DDV) of control module (CM) including the MCV receives the driving current input from the FLCC and drives the spool while delivering the LVDT voltage output to the FLCC.

With this MCV supply flow, power drive unit (PDU) generates the torque output while delivering the RVDT voltage output to the FLCC. Here, because the RVDT output should address the position of the flap, the FLCC should calibrate it and compare it with the RVDT output of the flap tip in real time. To transmit the torque, the torque tube receives the torque from the PDU, and transfers it to the RGAs. These RGAs deliver the driving torque to the flap while receiving the external air and inertial load and the RVDT attached to the end of the torque tube transfers the measured flap angle to the FLCC as a voltage simultaneously. Additionally, asymmetry brake module attached to the same position with the RVDT receives the input current from the FLCC. This asymmetry brake is operated electrically by receiving the driving current from the FLCC only when the position of the both wing flaps are in an asymmetrical position (i.e., asymmetry braking), and is operated mechanically only when the flap is driven above a certain speed. (i.e., overspeed braking). Now, in the following Sec.3-4, we will describe each part of the flap control system in detail and how it was modeled.

3. Flight Control System

This section describes the control layers of the FLCC. The FLCC consists of a high/low-level closed structure for processing the LVDT and RVDT sensor signals as shown in Fig.2. The model of FLCC in Sec. 3 is usually done by system manufacturer unlike that of the flap actuation and power transfer in Sec.4. Thus, it is necessary to overcome the difference of the interface from using different analysis tools because the softwares to be used can be different among manufacturers. In today's model based design [6-10], functional mock-up interface (FMI) is generally being applied for software interfacing and synthesis to overcome it. Typical performance analysis tools such as MATLAB/Simulink usually support the FMI.

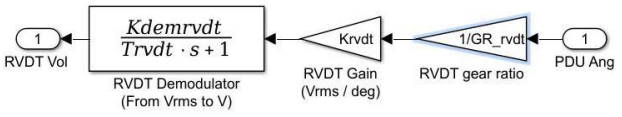

Fig. 3 RVDT Signal Transmission

3.1. Flap Angular Position Control

First, see the model of the RVDT. In Fig.3, the RVDT on PDU angle position is transformed into a root mean square (RMS) voltage value by the RVDT gear ratio and the RVDT gain (Vrms/deg), and is transmitted to the FLCC. This RMS voltage value is also converted through a low pass filter and a demodulator. The demodulator rectifies the sinusoidal signal, and the low pass filter generates a dc voltage that is proportional to the rectified signal. [11] The $K_{dem,rvdt}$ in Fig.3 corresponds to the dc gain and T_{rvdt} describes the time constant of the low pass filter.

When selecting T_{rvdt}, it should be guaranteed to follow the MCV spool motion at the intended bandwidth. [11] With the RVDT signal, the control voltage can be simply calculated by the error of the angle command value corresponding to this dc voltage and the reference value of the FLCC, and is transmitted to the current loop driver by being saturated for electrical stability of the hardware. Meanwhile, since the output of this RVDT is a measurement value at the PDU, the FLCC must calibrate the angle measurement difference between the PDU and the flap. To do this, by multiplying the conversion constant C as shown in the Fig.4, this difference can be compensated. The conversion constant is calculated as follows.

$$\text{Conversion} = \frac{GR_{RGA}}{GR_{RVDT} \cdot K_{rvdt} \cdot K_{dem,RVDT}} \tag{1}$$

where $\mathrm{GR}, K_{rvdt}, K_{dem,rvdt}$ denote gear ratio, RVDT resolution (Vrms/deg), and RVDT demodulator gain respectively. From the above calculation, you can know that the FLCC's conversion constant calibrates the measured value of the flap position that is expanded or contracted by the gear of RGA and RVDT. On the other hands, note that only the RVDT voltage output mounted on the PDU is utilized for controlling the position of the flap. Even though the flap position is directly transferred to the FLCC by RVDT mounted on the flap tip, the reason for using the RVDT value at the PDU in the main control layer

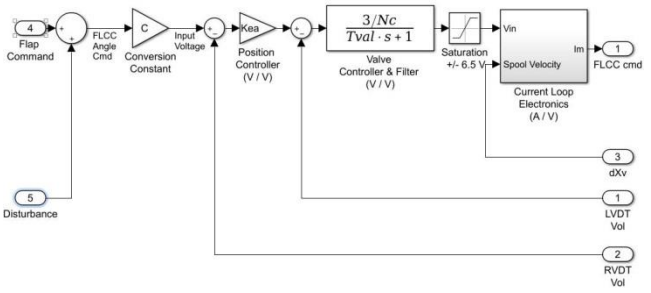

Fig. 4 Flight Control Computer

is that the distance from the PDU to the FLCC is much closer than the distance from the flap tip to the FLCC so that a more physically stable wiring can be constructed. The wiring of the aircraft is selected in consideration of such physical stability.

3.2. MCV Spool Position Control

The Fig.5 shows a model that generates linear force. Here, K_i is the force constant of the motor. From the Fig.5, it can be confirmed that the force is amplified in proportion to the available channel number N_c and, that is, the force motor is operated by N_c parallel current loops. This indicates that the force motor is a wiring triplex structure that can be usually seen in the electric system. If a single wire fails in operation of a major part, it can't guarantee its proper operation. Therefore, triplex wiring is often used in the applications where safety is the top priority. In this paper, we distinguish making full performance by 3 coils and partial performance by 1 or 2 coils. In many practical mechanical systems, including aircraft, the system is designed by setting the operation requirements differently with respect to each 1-3 coils operation mode. According to the operating mode, in usual simulation, the current, which drives the force motor, is logically adjusted by system manufacturer. Meanwhile, this linear force of the force motor now moves the spool of the hydraulic valve, and thus the spool dynamics can be used as follows. (2-3)

$$M_{ddv}\ddot{x} + B_{ddv}\dot{x} + K_{ddv}x + F_f = F_m \tag{2}$$

$$F_f = 2 \cdot C_d.C_v.A \cdot (P_1 - P_2)\cos\theta \tag{3}$$

where F_f, F_m, x of Eq.(2) are flow force, generated force of force motor, and the position of spool respectively. $M_{ddv}, B_{ddv}, K_{ddv}$ indicate that the spool was modeled as simple mass-spring-damper system. Eq.(3) is a widely known flow force equation. [12]

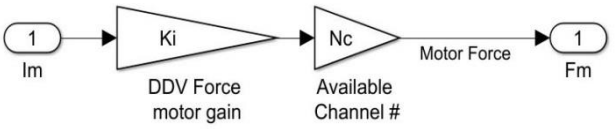

Fig. 5 DDM and Coil

Flow force is reaction force acting in the direction that interferes with flow, and is usually not negligible. In order to model the flow force, it is common to approach using the above Eq.(3), but the difference from the actual value is inevitable and must be calibrated through a lot of experiments. Finally, the FLCC model includes the current loop electronics in Fig.6. This loop reflects the generation of current by resistance and inductance, the PWM drive, and the reverse impact of back EMF voltage generation. Also, K_{imp} is also a hardware specification for addressing motor drive current and control voltage. In the following Sec.4, we will explain the model for hydraulic/mechanical parts in detail.

4. Hydraulic and Mechanical Components Modeling

The hydraulic motor generates torque by the flow rate controlled by FLCC and the generated torque is transmitted along the flap surface to mechanically actuate the flap. See Fig.7-8. Hydraulic and mechanical components model is sequentially constructed by considering flow valve model, flow continuity of hydraulic motor, torque equilibrium, motor dynamics, and flap kinematics. In addition, if a detailed model of the flap that can reflect the external load locally is constructed, the variation of flap motion along the aircraft's hinge line can be addressed.

4.1. Hydraulic Control Valve and Power Drive

First, the MCV can be solved by the following equation (4-5)

$$Q_L = \frac{C_{d,p}C_{d,r}}{\sqrt{{C_{d,p}}^2 + {C_{d,r}}^2}} \cdot w \cdot x \cdot \sqrt{\frac{2}{\rho}(P_s - P_r - P_L - P_{loss})} \quad (4)$$

$$P_L = (P_{C1} - P_{C2} - P_{loss}) - \frac{\rho}{2}\left[\left(\frac{1}{C_{d,p}}\right)^2 + \left(\frac{1}{C_{d,r}}\right)^2\right] \cdot \left(\frac{Q_L}{w \cdot x}\right)^2 \quad (5)$$

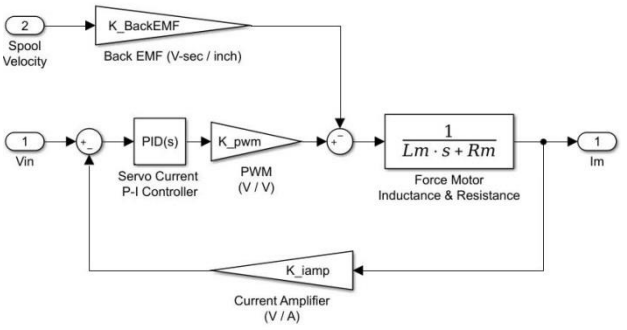

Fig. 6 Current Loop Electronics

where $C_{d,p}, C_{d,r}$ are supply, return flow coefficient and P_s, P_r, P_L, P_{loss} are supply, return, load pressure, and line loss respectively. The Eq.(4) is nothing but orifice equation and Eq.(5) is load pressure equation of MCV. Note that the slot area of Eq.(4) is a rectangle. In the case of aircraft, the MCV port is designed as a rectangular slot despite the difficulty in manufacturing the valve for actuators such as flaperon, horizontal tail, rudder, flap, etc. [12] Meanwhile, the sum of square slot widths in the radial direction is called the area gradient w. By adjusting the area gradient, the flow rate can be controlled linearly. [12] Designing the area gradient of the MCV port to meet the flow rate or the speed requirement is the most important part of the MCV design. This controlled flow rate is generally directed to the hydraulic motor through a fail-safe valve (FSV). Designing the FSV, various losses from passing through the FSV must be considered while addressing the main function of the fail-safe valve, which is to switch on-off for fail/operation.[13] However, note that this detail consideration is valid to the case where detailed analysis is required for component development at the part level. At the system level design, the FSV model can be included for the purpose of examining whether the fail-safe function is properly implemented in the failure mode. On the other hands, the analysis model can be elaborated more precisely as the details including the loss originated from clearance at the MCV, the change in viscosity and density with respect to temperature change, and etc. are included. In our study, the model doesn't include a FSV and corresponds to a system model which doesn't reflect the detailed design of the MCV. While this system model is sufficient to inspect the overall system performance, it's difficult to utilize it for the detailed

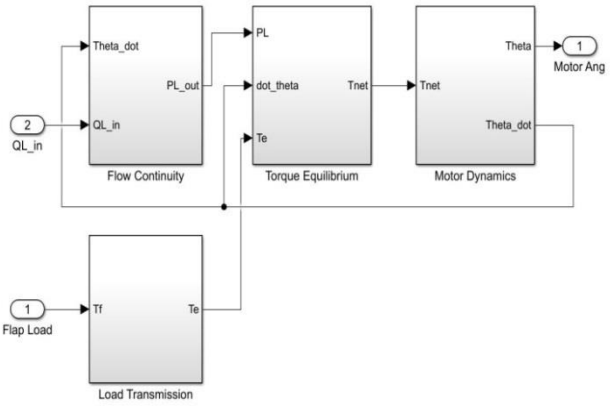

Fig. 7 Hydraulic Motor and PDU Subsystem

design of each part. Therefore, if engaged in the specific part development, it needs to build the model by separating that part only. However, in terms of overall system design, it's appropriate to construct a system model, extract the whole system performance, develop a detailed model of each part, and plug-in the existing model sequentially. In order to accurately reflect the irregular elements of the actual design, experiments that can be quantitatively compared should be done in parallel. The detailed model of the valve itself will be discussed later and will be omitted in this paper.

$$Q_L = D_m\dot{\theta}_m + \frac{C_s D_m}{\mu} P_L \tag{6}$$

$$C_s = \frac{\mu}{D_m}(\mathrm{C}_{im} + C_{em}) \tag{7}$$

where Q_L, D_m, μ of Eq.(6) are motor flow, motor displacement, and dynamic viscosity respectively.[12] $\dot{\theta}_m$ is the rotational velocity of the motor. Eq.(6) shows the flow continuity between CM and hydraulic motor. The first term of Eq.(6) indicates the transfer of the ideal flow rate by the motor, and the second indicates flow leakage. Eq.(7) defines the leakage coefficient C_s. The C_{im}/C_{em} of Eq.(7) indicate the internal/external leakage including the case drain of the hydraulic motor. Note that the second leakage term of Eq.(6) contains μ. That is, the leakage of the hydraulic motor depends on the fluid temperature. Meanwhile, the generated flow Q_L through the hydraulic motor generates torque as follows.[12]

$$\tau = D_m P_L - C_v D_m \mu \dot{\theta}_m - \frac{\dot{\theta}_m}{|\dot{\theta}_m|} C_f D_m P_s - \tau_e \tag{8}$$

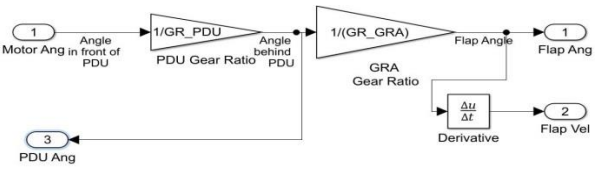

Fig. 8 Flap Kinematics

where C_v, C_f, τ_e indicate viscous friction, internal friction, and external load respectively. Meanwhile, in our research, the flow rate through the motor is fixed when the motor turns once. (i.e, a fixed displacement motor) The first term of Eq.(8) denotes the ideal torque, which is generated by the pressure difference across the motor, and the second and third terms are the viscous damping and the internal friction term of the hydraulic motor respectively. From Eq.(8), note that the viscous damping friction term is proportional to the dynamic viscosity μ. The relation between the temperature of hydraulic fluid and μ is usually logarithmic, so torque loss increases very much at extreme low temperatures. As mentioned above, when the temperature is lowered and the viscosity increases, both leakage and torque loss is increased. Therefore, when designing aircraft actuators, an appropriate operating temperature range should be set in consideration of this problem. In actual development process, the design of aircraft system/components consider the change of performance with respect to the temperature change by setting the temperature range that can give full performance (e.g., output speed, load capacity, etc.) In most cases, this is a very sensitive issue.

4.2. Power Transmission and Flap Actuation

The torque generated by Eq.(8) is transferred through the torque tube to several RGAs located on the flap surface to actuate the flap. See Fig.8 and the simple calculation below.

$$\theta_{flap} = \frac{\theta_m}{GR_{PDU} \cdot GR_{RGA}} \tag{9}$$

The angular position of the hydraulic motor is reduced by the gears of the PDU and RGA while determining the angular position and velocity of the flap. On the other hand, as you can see from the Eq.(9), this paper focuses on the reduced rate due to the gear of RGA and PDU and does not deal with the torque transmission to the flap, and its load distribution. In other words, this system analysis

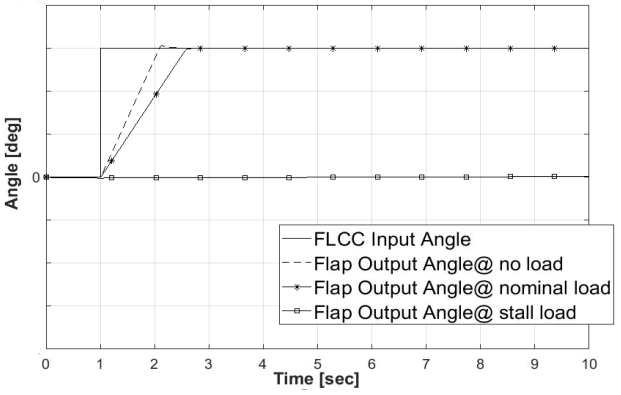

Fig. 9 Flap Angle at no load/nominal load/stall load

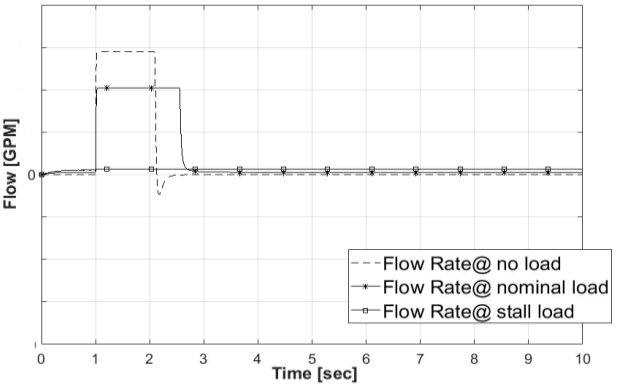

Fig. 13 Flow Rate at no load/nominal load/stall load

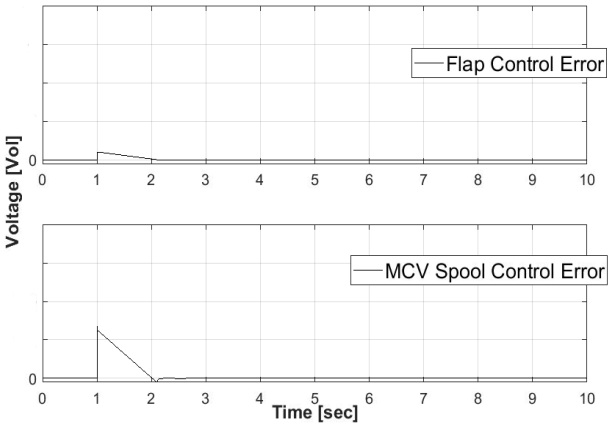

Fig. 10 Control Performance at no load condition

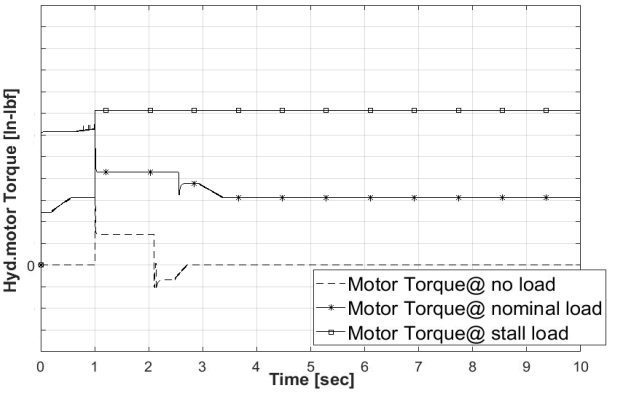

Fig. 14 Motor Torque at no load/nominal load/stall load

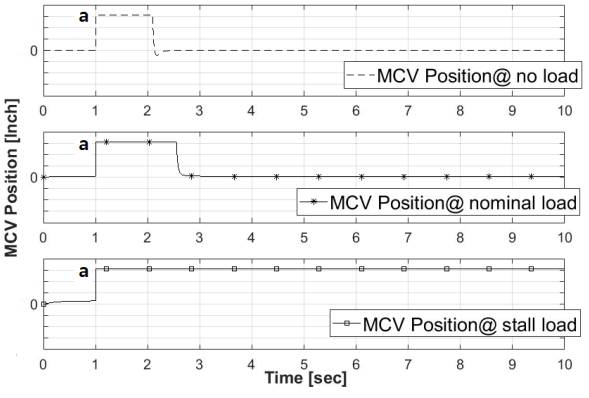

Fig. 11 MCV position at no load/nominal load/stall load

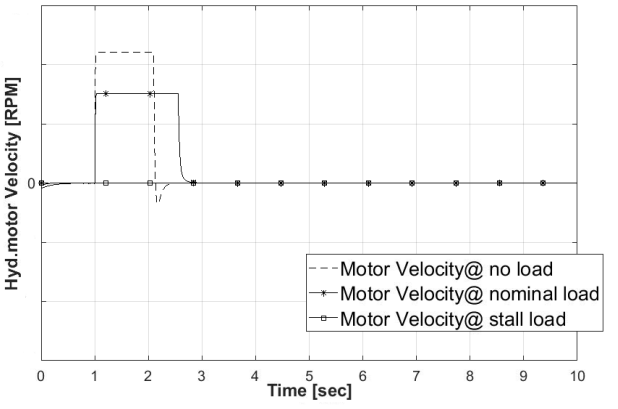

Fig. 15 Motor Velocity at no load/nominal load/stall load

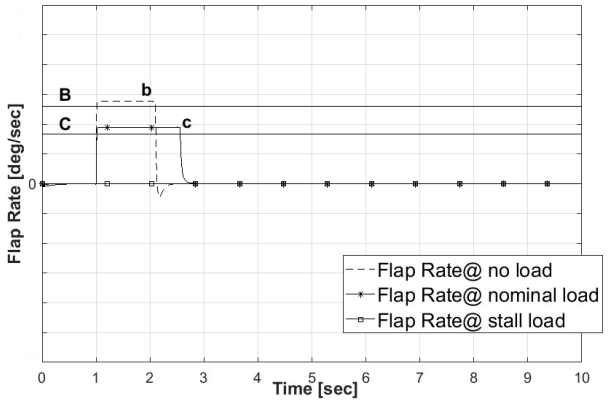

Fig. 12 Flap Rate at no load/nominal load/stall load

model focuses on the kinematics that is transmitted from the hydraulic motor to the flap surface and does not consider the dynamics of the torque tube and flap. In this way, the analysis of the motion along the flap surface in Sec.4.2 is interpreted by the simplified kinematic model, since the system load is taken into account by the external load τ_e all at once in Eq.(8), there is no problem in confirming the main performance of the flap. To see the motion of each RGA separately, each RGA should be modeled and its position must be determined separately in advance.

Meanwhile, the each RGA actuates the flap

together while having its structural limit load to enable movement of the flap. In general, the certain hinge moment along flap surface is given as the system requirement and the limit load sum of several RGAs along the flap surface is structurally safe only if it exceeds the requirement. Thus, it is important to select the number and position of RGAs appropriately while considering the inertial and aerial hinge load and the design should proceed with sufficient margin. We will deal with complicated models of power transmission of flap in future.

5. Simulation Results

Now, we will provide the result on the simulation for flap actuation. Note that, because of confidentiality of the business of defense, we randomly selected the certain values of simulation and concealed the several results with letters such as a, b, and so on. For testing of our model, we performed three cases of no load, nominal, and stall external load, and the results are shown in Fig.9-15.

In Fig.9-15, we commonly gave 30 deg command as reference input and you can see that the flap angle commonly goes to the reference angle in Fig.9. After moving to the reference angle, the flap is almost completely stopped by the flight control even though small oscillation of the flap is found. The control performances of the higher/lower control layer are shown in Fig.10. While the flap is operating, you can also confirm that the MCV spool is opened as much as the maximum available displacement 'a' in Fig.11. This spool displacement 'a' can be solved by Eq.(2) and the valve is closed after the flap goes to the desired position. Due to the external load, the maximum displacement time of loaded cases is larger than that of no load case. On the other hands, the angular velocity of the flap is designed to meet the no load/nominal performance requirements 'B', 'C', which can be confirmed in Fig.12. You can see that the resultant flap velocity 'b', 'c' satisfy the no load, nominal velocity requirements 'B', 'C' respectively and the velocity at stall condition is almost stopped. Meanwhile, in Sec.4.1, the flow rate of hydraulic domain passes to the hydraulic motor through the MCV by the motion of spool. This flow rate, which is shown in Fig.13, is calculated by Eq.(4-7). You can see that the flow rate at no load is the largest, and the flow rate decreases as the external load increases. For the generation of mechanical power, the flow rate forms the mechanical torque by the hydraulic motor while the viscous and internal friction in Eq.(8) are considered. The generated torque by the motor is seen in Fig.14. From the figure, you can see that, while the generated torque is the smallest in case of no load condition, it's the largest in case of stall load condition. Additionally, at no load point during flap operation (i.e., 1-2 sec), you can also confirm that the generated torque isn't zero due to viscous, internal friction torque in Eq.(8). Thus, the rotational velocity of motor in Fig.15 can be obtained by differentiating its acceleration and, from the figure, you can confirm that the velocity of motor decrease as the external load increases. This is due to the fact that the flap is less turned by the external load and therefore the flow rate is low, which is consistent with the theoretical explanation. Finally, this resultant rotational velocity of the motor is transmitted to the flap, which is solved by the kinematics (9), and the its positon is again returned to the FLCC by RVDT as described in Sec.2

Table 1 Flap Performance Variation with respect to Temperature Change

	No load Rate (deg/sec)	Nominal Rate (deg/sec)	Stall Load (in-lbs)
36°F	0.724α	0.760β	1.001γ
100°F	α	β	γ
275°F	1.096α	1.143β	1.002γ

Next, we will investigate the flap's performance change according to the temperature variation. As described in Sec. 4.1, as the temperature decreases, the effect of viscosity on the performance of flap is absolute although both viscosity and density change. To confirm this, we performed the simulation at 36, 100, and 275 °F.

See Table.1. Table.1 shows comparison of no load rate, nominal rate, and stall load at 36, 100, and 275 °F. Based on the result at 100 °F, we represent the no load flap velocity, nominal flap velocity, and stall load at 100 °F as α, β, and γ respectively. In Table.1, you can find that there is a same tendency for the flap velocity when the temperature changes. If the temperature decreases, the flap velocity also decreases. This tendency can be described by Eq.(6) and (8). That is, when the temperature decreases,

the effect of flap rate reduction due to the torque reduction in Eq.(8) is far greater than the effect of flap rate increase due to leakage reduction in Eq.(6). Therefore, determining the coefficient C_s in Eq.(6) and C_v in Eq.(8) is imperative for examining the temperature influence on system performance. We experimentally concluded that the temperature influence is strongly dependent on C_v .

Despite the protection of the parameters, variables, and results for security reasons, we can say that these are meaningful results in that it meets key requirements by model-based engineering from the perspective of the whole system. Along with that point, we can confirm that the correlation among the external load, resultant torque, and flow rate is consistent with the theoretical description.

6. Summary and Future Work

In this research, we represented the results on the performance analysis model that reflects the actual aircraft's flap control system and confirmed that the results are reasonable. By utilizing this Simulink model, we can see the change of flap behavior while analyzing the effect of design parameter. In future, we need to complement the followings to our performance analysis model:

1) Reflect the detailed design for the each part (i.e., MCV, FSV, etc.)
2) Construct the complicated dynamics model for flap actuation and power transmission.
3) Realize the rest of redundant components that have fail-safe function (e.g., Asymmetry brake)
4) Develop an evolved model that can be used for model based design rather than system analysis.
5) Verify the model by real implementation

The results of this study can be applied to the construction of the performance analysis model of other aircraft flaps. If more sophisticated model can be built, we think that it can be used more actively in future model-based engineering.

References

[1] H. Cho, I. Lee, S. Kim, S. Park, M. Yang, "No-Failure Accelerated Life Test of Flap Actuating System using Weibull Distribution", *Journal of the Society for Aerospace System Engineering*, vol. 10, no. 1, pp. 51-58. Mar. 2016.

[2] Y. Nam and H. Park, "Analysis on the dynamics characteristics of a DDV actuation system of a FBW Aircraft", *Journal of the Korean Society for Aeronautical and Space Sciences*, vol. 34, no. 3, pp. 74-80, Mar. 2006

[3] M. Park, Y. Kim, and E. Kim, "Trend of Fly-By-Light Technology Development", Aerospace Engineering and Technology, vol. 5, no. 1, pp.49-56, July. 2006.

[4] G. Yoon, H. Park, and K. Jang, "The state of the art and application of actuator in Aerospace", *Journal of the Korean Society of Propulsion Engineers*, vol. 14, no. 6, pp.89-102, Dec. 2010.

[5] D. Crane, *Dictionary of Aeronautical Term*, 5th Ed., Aviation Supplies and Academics, Inc., Newcastle, 2012

[6] Y. Kim, H, Yoon, and S, Kim, "A Model-based design and testing approach for the UAV flight control computer", *Proc. of the Korean Society for Aeronautical and Space Sciences 2015*, Jeongseon, Korea, pp.620-633, Apr. 2015.

[7] H. Park, S. Jang, S. Baek, and J. Byun, "HILS simulation model integration guidelines using Model-based design and MATLAB Simulink", *Proc. of the Korean Society for Aeronautical and Space Sciences 2016*, Jeju, Korea, pp.796-797, Nov. 2016.

[8] D. Han, Y. Kim, C. Lee, D. Lee, and K. Cho, "A study on verify of UAV flight control software simulated flight using Model-based development and X-plane simulator", *Journal of the Korean Society for Aeronautical and Space Sciences*, vol. 43, no. 2, pp.166-171, Feb. 2015

[9] C. Joo, "Model design for performance analysis of leading-edge flap actuation system", *Proc. of the SASE Fall Conference 2016*, Muju, Korea, Nov 2016

[10]R. L. Tovo, F. J. Vargas, and L. C. S. Goes, "Creation of virtual environment with AMESim and its Integration with MATLAB/Simulink", *Proc. series of the Brazilian Society of Computational and Applied Mathematics*, vol. 4, no. 1, Oct. 2016

[11]R. C. Dorf and R. H. Bishop, *Modern Control Systems*, 12th Ed., Prentice-Hall, 2010.

[12]H. E. Merritt, *Hydraulic control systems*, 1st Ed., John Wiley & Sons, Inc., 1991.

[13]N. Su, T. Kim, K. Kim, and S. Park, "Design fail-safe valve for leading edge flap of aircraft", *Proc. of the Korean Society for Aeronautical & Space Sciences 2016*, Jeju, Korea, pp.840-842, Nov 2016